Temperature- and water-induced structural transformations in Ba(Ce$_{0.7}$Zr$_{0.1}$Y$_{0.1}$Yb$_{0.1}$)O$_{3–δ}$ proton conducting electrolyte

Ivan Ivanov [ab] * [iD], Dmitry Tsvetkov [ab] [iD], Vladimir Sereda [ab] [iD], Dmitry Malyshkin [ab] [iD], Anna Sereda [a] [iD], Petr Zakiryanov [a] [iD], Roman Yagovitin [ab] [iD], Andrey Zuev [a] [iD]

a: Institute of Natural Sciences and Mathematics, Ural Federal University, Ekaterinburg 620002, Russia
b: Institute of Chemical Engineering, Ural Federal University, Ekaterinburg 620009, Russia
* Corresponding author: ivan.ivanov@urfu.ru
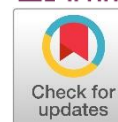
This paper belongs to a Regular Issue.

Abstract

The crystal structure of Ba(Ce$_{0.7}$Zr$_{0.1}$Y$_{0.1}$Yb$_{0.1}$)O$_{3–δ}$ was studied depending on temperature in dry and wet atmosphere using in situ high temperature X-ray powder diffraction. Phase transition from tetragonal $I4/mcm$ to cubic $Pm\bar{3}m$ structure was shown to occur in Ba(Ce$_{0.7}$Zr$_{0.1}$Y$_{0.1}$Yb$_{0.1}$)O$_{3–δ}$ upon heating from 25 up to 1000 °C irrespective of air humidity. The cubic $Pm\bar{3}m$ and tetragonal $I4/mcm$ phases possess comparable coefficients of linear thermal expansion (CTEs), 10.6·10^{-6} K^{-1}. Even in very dry atmosphere (10^{-4} atm H$_2$O), chemical expansion caused by hydration contributes significantly to the observed structural transformations and the variation of the unit cell parameters of Ba(Ce$_{0.7}$Zr$_{0.1}$Y$_{0.1}$Yb$_{0.1}$)O$_{3–δ}$.

Key findings

- Phase transition from tetragonal $I4/mcm$ to cubic $Pm\bar{3}m$ structure occurs in Ba(Ce$_{0.7}$Zr$_{0.1}$Y$_{0.1}$Yb$_{0.1}$)O$_{3–δ}$ upon heating.
- Hydration influences the unit cell size and symmetry of Ba(Ce$_{0.7}$Zr$_{0.1}$Y$_{0.1}$Yb$_{0.1}$)O$_{3–δ}$ even in dry atmosphere.
- Coefficients of thermal and chemical expansion were determined for Ba(Ce$_{0.7}$Zr$_{0.1}$Y$_{0.1}$Yb$_{0.1}$)O$_{3–δ}$.

Supplementary materials
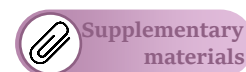
1. Introduction

Various substituted barium zirconates and cerates with a perovskite-type structure are the-state-of-the-art proton-conducting electrolyte materials for protonic ceramic fuel cells (PCFCs). Compared to cerates, zirconates possess lower protonic conductivity but higher stability in H$_2$O and CO$_2$ containing atmospheres. Hence, it is not surprising that BaCe$_{1-x}$Zr$_x$O$_{3–δ}$ (BCZ) solid solutions were found to be a good compromise between stability and functional properties for PCFC applications [1]. Further substitution of rare earth metals, such as Y and Yb, for Ce in BCZ, as was shown by Yang et al. [2], promotes higher protonic conductivity and better material stability in hydrocarbons and hydrogen sulfide containing atmosphere. In particular, the composition Ba(Ce$_{0.7}$Zr$_{0.1}$Y$_{0.1}$Yb$_{0.1}$)O$_{3–δ}$ (BCZYYb7111), which is the focus of this work, demonstrated excellent performance as an electrolyte in PCFCs [2].

It is generally recognized that comprehensive understanding of the crystal structure of an electrolyte material is of key importance for its successful application. However, the crystal structure of BCZYYb7111 still remains a controversial topic, since even at room temperature (RT) it was described using $Imma$ [3–8], $Pbnm$ [9] or $I4/mcm$ [10] space group (s. g.). In all these cases the distortion of the ideal perovskite-type cubic lattice with s.g. $Pm\bar{3}m$ results from the cooperative tilting of the (Zr,Ce,Y,Yb)O$_6$ octahedra [10]. The Zr,Ce,Y,Yb – cations are believed to be randomly distributed within the octahedra with an average (Zr,Ce,Y,Yb)–O distance of 2.219 Å.

The phase transitions in BCZYYb7111 were investigated [1] using high-temperature X-ray diffraction (HT XRD) in controlled atmospheres on cooling from 900 to 25 °C. The crystal structure of BCZYYb7111 was found to depend on the atmosphere: while the samples prepared in air exhibited two consecutive phase transitions (cubic $Pm\bar{3}m$ → trigonal

$R\overline{3}c \rightarrow$ monoclinic $I2/m$) upon cooling, the dehydrated BCZYYb7111 prepared by calcining at 1000 ºC in dry N_2 was found to remain trigonal ($R\overline{3}c$ s. g.) in dry N_2 down to RT [1]. Zhang et al. [9] also reported the existence of two phase transitions in BCZYYb7111. The higher-temperature one from cubic $Pm\overline{3}m$ to trigonal $R\overline{3}c$ structure is the same as the one reported in [1], whereas at lower temperatures the transition to orthorhombic $Pbnm$ instead of monoclinic phase was found. On the contrary, Hamze et al. [10] using powder X-ray and neutron diffraction showed that only one phase transition occurs upon heating in BCZYYb7111. At RT, it possesses the tetragonal structure with $I4/mcm$ s. g., which continuously transforms to the cubic one with $Pm\overline{3}m$ s.g. upon heating due to the reduction of the tetragonal distortions. When analyzing the reasons for disagreement between the abovementioned results, one should remember that for hydratable phases, such as the proton conducting oxide BCZYYb7111, the actual hydration degree of the sample and the water vapor pressure in the surrounding atmosphere must be taken into account for correct interpretation of the experimental evidences. Noteworthy in this respect is that in the works [9, 10] neither of these was controlled.

Taking into account all mentioned above, the present study was aimed at investigating the crystal structure of BCZYYb7111 depending on temperature in dry and wet atmosphere using in situ high temperature X-ray powder diffraction supplemented by thermogravimetric (TG) measurements. This work was performed to resolve the existing discrepancy in the literature data [1, 9, 10] and gain new insights into the thermal and compositional dependence of the crystal structure of state-of-the-art proton conducting oxides.

2. Experimental

The powder samples of BCZYYb7111 were synthesized via the standard ceramic method using Y_2O_3, Yb_2O_3, CeO_2, $BaCO_3$ and $Zr(OH)_2CO_3$ as the starting materials, whose purity and suppliers are listed in Table 1. $BaCO_3$ was preliminary calcined at 450 ºC to remove the adsorbed H_2O and CO_2. Y_2O_3, CeO_2 and Yb_2O_3 were preliminary calcined at 1100 ºC to remove the adsorbed H_2O. The starting materials were mixed in the required stoichiometric amounts with the sintering additive (1 wt.% of NiO) followed by grinding.

Table 1 The source and purity of the starting materials.

| Chemical name	Source	Mass fraction purity	Analysis method
$BaCO_3$	Lanhit	>0.9999	*
$Zr(OH)_2CO_3$	ChMZ	>0.9999	*
CeO_2	Lanhit	>0.99	*
Y_2O_3	Vekton	>0.99	*
Yb_2O_3	Vekton	>0.99	*
NiO	Vekton	>0.99	*
BCZYYb7111	Synthesis	>0.99	XRD, SEM EDX

* vendor statement

Afterwards, the as-synthesized powders were uniaxially pressed at 154 MPa into tablets 20 mm in diameter and were covered with the sacrificial powder of the same chemical composition in order to prevent Ba loss during subsequent thermal treatment. The tablets prepared accordingly were heated with the rate of 300 K·h⁻¹ up to 1500 ºC in air, annealed at this temperature for 10 hours, and then cooled with the rate of 100 K·h⁻¹ down to room temperature. The sintered tablets were crushed in an agate mortar to obtain the powder for the subsequent measurements.

The XRD patterns were recorded with a 7000S (Shimadzu, Japan) X-ray diffractometer using Cu Kα radiation. In situ high-temperature XRD measurements (HT XRD) were carried out using the same diffractometer equipped with a high temperature chamber HTK 1200N (Anton Paar, Austria). The humidity and oxygen partial pressure in the atmosphere employed in the HT XRD measurements was controlled using homemade setup based on mass flow controllers RRG12 (Eltochpribor, Russia) shown in Figure 1 by mixing the flows of dry and humidified gaseous N_2 and air in the appropriate ratios. The gases were dried to the residual water vapor pressure of $\log(p_{H_2O}/atm) = -4.0$ by passing them through the zeolite column. The humidified gases with water vapor partial pressure up to $\log(p_{H_2O}/atm) = -1.7$ were prepared by bubbling through water thermostated at 1–50 ºC with an accuracy of 0.05 ºC. Oxygen partial pressure (p_{O_2}) around the sample was controlled by a universal controller, Zirconia 318 (Russia), with YSZ-based potentiometric sensor.

The humidity of the gas (i.e., p_{H_2O}) was measured using the original unit based on the H_2O-sensor BME-280 (Bosch, Stuttgard, Germany). Before recording the XRD pattern, the sample was equilibrated at each given p_{O_2}, p_{H_2O} and T for at least 6 h.

Water uptake of the BCZYYb7111 sample was measured by the thermogravimetric technique (TG) using CI Precision (UK) microbalances. The measurements were carried out in the temperature range 25–900 ºC in dry $(\log(p_{H_2O}/atm) \leq -4)$ and wet $(\log(p_{H_2O}/atm) = -1.7)$ air. The sample was equilibrated at each temperature and pH₂O for, at least, 2 h until reaching a constant weight.
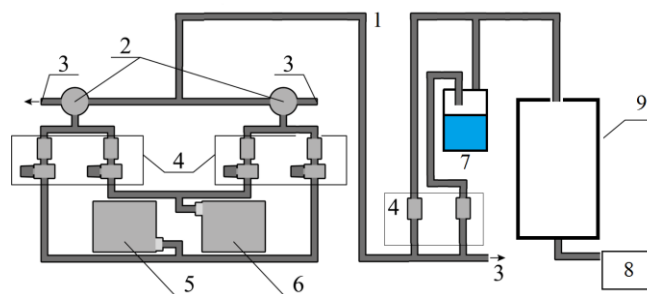
Figure 1 Schematic drawing of the gas mixing unit: 1 – gas tube (304 steel), 2 – 3-way electrical valve (SMC, Japan), 3 - check valve (SMC, Japan), 4 – mass flow controllers, 5 – dry air compressor, 6 – nitrogen generator, 7 – water thermostat, 8 – p_{H_2O} sensor BME-280 (Bosch, Stuttgard, Germany) and p_{O_2} sensor Zirconia 318 (Russia), 9 – HTK 1200N.

However, under dry air atmosphere the equilibration kinetics was so slow that only rough estimates of the water uptake could be determined, for example, at 400 °C even 300 h equilibration was not enough, and sample's weight was still increasing.

3. Results and Discussion

The XRD analysis of the as-prepared BCZYYb7111 sample showed no evidence of the presence of any secondary phase. The XRD pattern was indexed using the $I4/mcm$ space group and is shown in Figure 2 along with the Rietveld refinement results.

The HT XRD patterns of BCZYYb7111 recorded at temperatures between 1000 °C and RT in dry ($\log(p_{H_2O}/atm) = -4.0$) and wet air ($\log(p_{H_2O}/atm) = -1.7$) are shown in Figures 3 and 4, respectively. The phase transition in BCZYYb7111 is clearly observed upon cooling in both dry and wet air. As seen, in dry air BCZYYb7111 possesses the cubic $Pm\overline{3}m$ structure at relatively high temperatures in the range of $700 \leq T, °C \leq 1000$ (Figure 3), whilst this range narrows a little in wet air, where the $Pm\overline{3}m$ structure is stable only down to 800 °C. At the low limit of the $Pm\overline{3}m$ structure stability, the crystal lattice of BCZYYb7111 transforms to the tetragonal one with $I4/mcm$ s.g., which remains stable upon further cooling down to RT.

To confirm the suggested sequence of the structural transitions, the Rietveld-refined XRD patterns recorded for BCZYYb7111 at 600 and 1000 °C in dry air and at 600 and 1000 °C in wet air are given in Figures 5 and 6, and in Supplementary (Figures S1–S2, respectively).
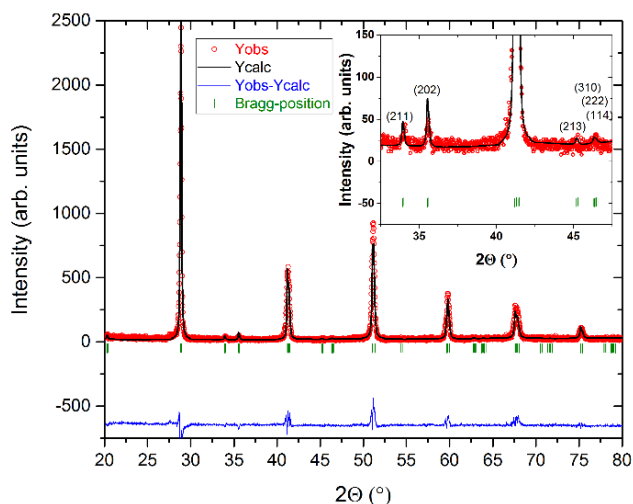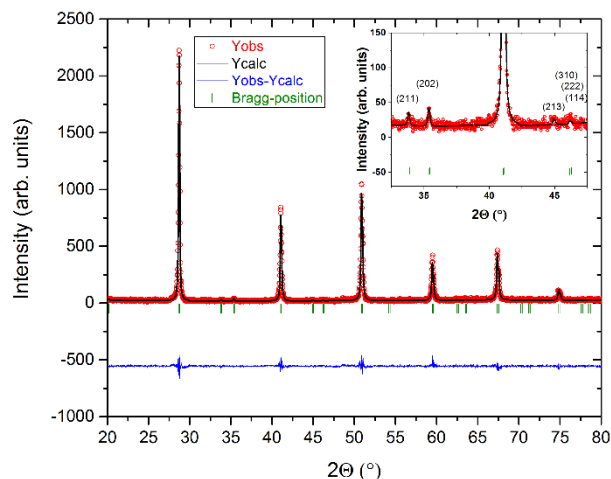

Figure 2 Refined XRD pattern, recorded at RT, of BCZYYb7111 sample ($I4/mcm$ s.g.) slowly (100 °C·h⁻¹) cooled from 1500 °C down to RT in dry air ($\log(p_{H_2O}/atm) = -4.0$): observed X-ray diffraction intensity (°) and calculated curve (−). The bottom curve (−) is the difference between the observed and calculated patterns, $y_{obs}-y_{cal}$, and the small blue bars (|) indicate the angular positions of the allowed Bragg reflections. The inset shows the zoomed part of the refined pattern in the range of $32.5 \leq 2\theta, ° \leq 47.5$ along with the Miller indices of the allowed reflections.
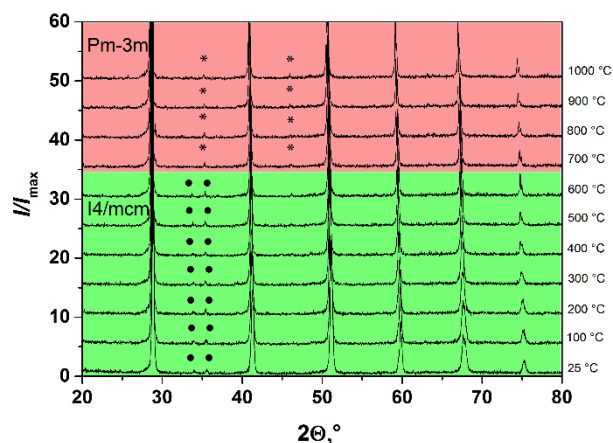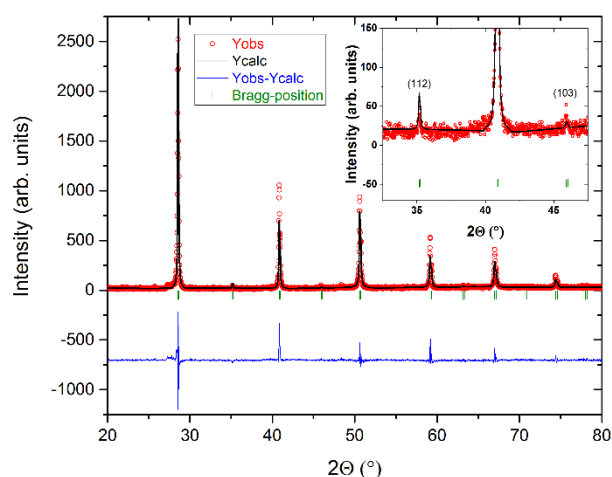

Figure 3 XRD patterns of BCZYYb7111 sample recorded at temperatures between 1000 °C and RT in dry air, $\log(p_{H_2O}/atm) = -4.0$. * and ● symbols correspond to the characteristic reflections of cubic $Pm\overline{3}m$ and tetragonal $I4/mcm$ structures, respectively.
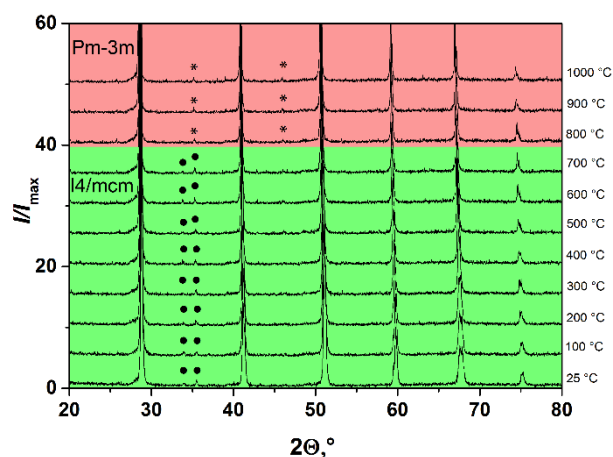
Figure 4 XRD pattern of BCZYYb7111 sample recorded at temperatures between 1000 °C and RT in wet air, $\log(p_{H_2O}/atm) = -1.7$. * and ● symbols correspond to the reflections of cubic $Pm\overline{3}m$ and tetragonal $I4/mcm$ structures, respectively.

Figure 5 Refined XRD pattern, recorded at 600 °C, of BCZYYb7111 sample ($I4/mcm$ s.g.) in dry air ($\log(p_{H_2O}/atm) = -4.0$): observed X-ray diffraction intensity (°) and calculated curve (−). The bottom curve (−) is the difference between the observed and calculated patterns, $y_{obs}-y_{cal}$, and the small blue bars (|) indicate the angular positions of the allowed Bragg reflections. The inset shows zoomed part of the pattern in $32.5 \leq 2\theta, ° \leq 47.5$ along with Miller indices.

Figure 6 Refined XRD pattern, recorded at 1000 ºC, of BCZYYb7111 sample ($Pm\bar{3}m$ s.g.) in dry air (log (p_{H_2O} / atm) = −4.0): observed X-ray diffraction intensity (º) and calculated curve (—). The bottom curve (—) is the difference between the observed and calculated patterns, $y_{obs} - y_{cal}$, and the small blue bars (|) indicate the angular positions of the allowed Bragg reflections. The inset shows zoomed part of the pattern in 32.5 ≤ 2Θ,º ≤47.5 along with Miller indices.

Thus, the findings of the present work support the conclusions of Hamze et al. [10] that at RT BCZYYb7111 possesses the tetragonal $I4/mcm$ structure which continuously transforms to the cubic one $Pm\bar{3}m$ upon heating due to the suppression of the cooperative tilting of the (CeZrYYb)O$_6$ octahedra in BCZYYb7111.

The phase transition temperature in BCZYYb7111, estimated in [10] to be 655(8) ºC in dry atmosphere (cubic $Pm\bar{3}m$ → tetragonal $I4/mcm$), is in perfect agreement with our results. As seen in Figures 3 and 7 according to our data the transition occurs in the temperature range 600–700 ºC at log (p_{H_2O} / atm) = −4.0 i.e. roughly at around 650 ºC. We did not confirm the presence of the second phase transition at lower temperatures reported in [1, 9].

The refined values of the unit cell parameters are summarized in Tables S1 and S2 (Supplementary information). The pseudo-cubic cell volumes depending on temperature in dry and wet air are shown in Figure 7. As seen, both phases have quite comparable linear CTEs (~10.6·10^{-6}).

The cell volume determined under wet atmosphere is higher than that under dry conditions due to the BCZYYb7111 sample hydration. Also of interest is its nonlinear temperature variation within the stability field of the tetragonal phase. Hamze et al. [10] suggested that the deviation from linearity of the tetragonal phase volume vs. temperature dependence is caused by a decrease of the equatorial B–O bond distance with temperature growth at $T < 700$ ºC in order to maintain the c/a ratio above 1. At 700 ºC, the slightly lower volume of the cubic cell was explained as a consequence of the convergence of equatorial and axial B–O bond distances [10]. All-in-all, this explanation attributes all the observed particularities of the thermal expansion of BCZYYb7111 solely to the temperature influence, disregarding the temperature variation of the hydration degree, which is an important feature of the proton conducting perovskite-type oxides.

At the same time, the results of our TG measurements presented in Figure 8 unambiguously show that even under very dry atmosphere, for example, that with log (p_{H_2O} / atm) = −4.0 used in this work, BCZYYb7111 hydrates upon cooling absorbing up to ca 0.027 mol H$_2$O per mol of the sample. This value can only be estimated approximately due to extremely slow equilibration kinetics in dry atmosphere at 400 ºC, so the equilibrium water content in BCZYYb7111 in these conditions is likely higher. At higher temperatures, however, the water exchange kinetics is faster, resulting in much lower uncertainties in the water content determination, as shown in Figure 8.

The temperature range of the most intensive hydration (see Figure 8) corresponds to that of nonlinear variation of the unit cell parameters of the tetragonal phase (see Figure 7). Hence, the chemical expansion upon hydration superimposed on the thermal expansion of BCZYYb7111 also contributes to the observed nonlinearity of the temperature dependence of its unit cell parameters even in dry air.
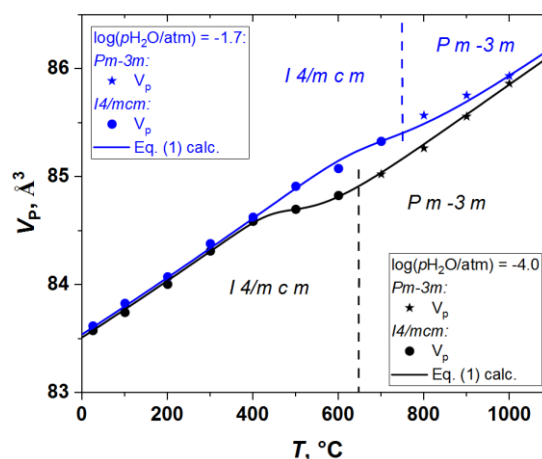
Figure 7 Pseudo-cubic cell volume of BCZYYb7111 versus temperature in wet (log (p_{H_2O} / atm) = −1.7) and dry (log (p_{H_2O} / atm) = −4.0) air. Symbols – values calculated using Rietveld-refined unit cell parameters, lines – result of calculations according to Equation (1).
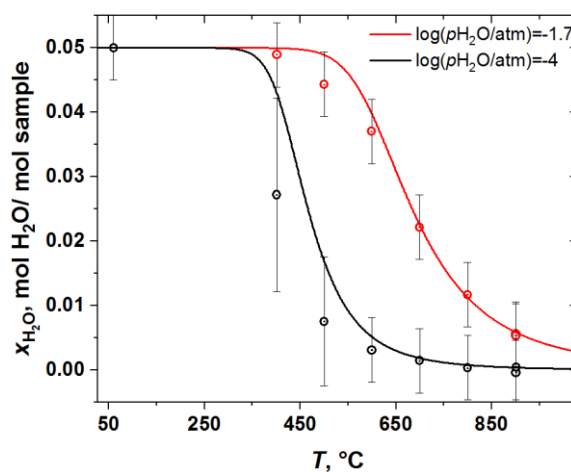
Figure 8 The hydration degree of BCZYYb7111 versus temperature in wet (log (p_{H_2O} / atm) = −1.7) and dry (log (p_{H_2O} / atm) = −4.0) air. Symbols – experimental values determined by TG, lines – guide to the eye. Note that under wet conditions the results are close to equilibrium whereas under dry conditions only estimates are given due to slow equilibration kinetics.

To support this conclusion, we estimated the variation of the pseudo-cubic lattice volume with temperature. According to the approach described in [11] the change in the sample's length is a sum of thermal and chemical contributions. Hence, for cubic or quasicubic lattice one can obtain the following equation:

$$V(T) = V_0 + 3\alpha_L(T - T_0) + 3\beta_L(x_{H_2O} - x^0_{H_2O}), \qquad (1)$$

where V_0 is the volume of the sample at the reference temperature T_0, α_L is the linear CTE, β_L is the linear chemical expansion coefficient, T is the temperature, T_0 is the reference temperature, and x_{H_2O} and $x^0_{H_2O}$ are the hydration degrees at T and T_0, respectively. T_0 = 1000 ℃ was selected as the reference temperature because the hydration degree at that temperature under dry conditions is essentially zero, i.e. $x^0_{H_2O}$ = 0. Therefore, V_0 corresponds to 1000 ℃ and $\log(p_{H_2O} / atm) = -4.0$. Chemical expansion coefficient (per mol of H_2O) was estimated according to the model described in [11] as β_L = 0.0317. For thermal expansion coefficient, the value of $\alpha_L = 10.6 \cdot 10^{-6}$ K^{-1} found at $T \geq 700$ ℃ under dry conditions was employed; in fact, this value is almost the same as α_L that can be calculated for the low-temperature tetragonal phase of BCZYYb7111. The hydration degree of BCZYYb7111, directly measured by TG (see Figure 8), was used as x_{H_2O} in Equation 1. The as-calculated lattice volume is shown as a function of temperature in Figure 7 in comparison with the experimental values measured in two atmospheres. The good agreement is obvious. In fact, because α_L in Equation 1 was assumed to be constant, we can conclude that all the nonlinearity of the observed temperature dependence of the cell volume can be explained by the variation in the water content in the sample. Hence, hydration induced chemical lattice expansion cannot be ignored when analyzing phase behavior and thermal expansion of BCZYYb7111 and similar proton conducting oxides even under the "dry" conditions with very low humidity.

4. Limitations

To gain better understanding of the particularities of the phase transitions in BCZYYb7111 additional precise neutron diffraction measurements are still required supplied with careful control of temperature, water vapor partial pressure and equilibration kinetics as well as simultaneous hydration studies under precisely the same conditions.

5. Conclusions

BCZYYb7111 was shown to undergo continuous phase transition from tetragonal $I4/mcm$ to cubic $Pm\bar{3}m$ structure upon heating both in dry and wet air ($\log(p_{H_2O} / atm) = -4.0$ and -1.7, respectively) due to, most likely, suppression of the cooperative tilting of the (CeZrYYb)O_6 octahedra. The tetragonal $I4/mcm$ structure is stable upon heating from RT up to around 650 ℃ in dry air and 750 ℃ in wet air. Both cubic and tetragonal phases were shown to possess quite similar linear CTEs. At the same time, hydration induced chemical expansion was shown to strongly affect both the absolute values of the unit cell parameters and the shape of their temperature dependence even under dry atmosphere with water vapor pressure as low as 10^{-4} atm. Hence, the chemical expansion cannot be ignored when analyzing the phase behavior and apparent thermal (which is, in fact, thermochemical) expansion of proton conducting oxides similar to BCZYYb7111 studied in this work.

● Supplementary materials

This manuscript contains supplementary materials, which are available on the corresponding online page.

● Acknowledgments

None.

● Author contributions

Conceptualization: I.L.I., D.S.T.
Data curation: I.L.I., P.O.Z., D.A.M.
Formal Analysis: A.V.S., P.O.Z., D.A.M.
Funding acquisition: I.L.I.
Investigation: P.O.Z., D.A.M., R.E.Y.
Methodology: I.L.L., A.Y.Z., D.S.T.
Project administration: I.L.I., D.S.T.
Resources: V.V.S.
Software: V.V.S.
Supervision: I.L.I., D.S.T.
Validation: V.V.S., D.A.M.
Visualization: P.O.Z.
Writing – original draft: I.L.L., A.Y.Z., D.S.T.
Writing – review & editing: I.L.L., A.Y.Z., D.S.T., V.V.S.

● Conflict of interest

The authors declare no conflict of interest.

● Additional information

Author Scopus IDs:
    Ivan Ivanov, 7402503149;
    Dmitry Tsvetkov, 7005876095;
    Vladimir Sereda, 35337908400;

Dmitry Malyshkin, 56024131600;
Anna Sereda, 59231896700;
Petr Zakiryanov, 58028030300;
Roman Yagovitin, 57221789281;
Andrey Zuev 7006001998.

Website:
Ural Federal University, https://urfu.ru/en/.

References

1. Nomura K, Shimada H, Yamaguchi Y, Shin W, Okuyama Y, Mizutani Y. Phase Transitions, Thermal Expansions, Chemical Expansions, and CO2 Resistances of $Ba(Ce_{0.8-x}Zr_xY_{0.1}Yb_{0.1})O_{3-\delta}$ (x = 0.1, 0.4) Perovskite-Type Proton Conductors. J Electrochem Soc. 2022;169:024516. doi:10.1149/1945-7111/ac5480

2. Yang L, Wang S, Blinn K, Liu M, Liu Z, Cheng Z, Liu M. Enhanced sulfur and coking tolerance of a mixed ion conductor for SOFCs: $BaZr_{0.1}Ce_{0.7}Y_{0.2-x}Yb_xO_{3-\delta}$. Sci.2009;326:126–129. doi:10.1126/science.1174811

3. Mirfakhraei B, Ramezanipour F, Paulson S, Birss V, Thangadurai V. Effect of sintering temperature on microstructure, chemical stability, and electrical properties of transition metal or Yb-doped $BaZr_{0.1}Ce_{0.7}Y_{0.1}M_{0.1}O_{3-\delta}$ (M=Fe, Ni, Co, and Yb). Fron Energy Res. 2014;2:9. doi:10.3389/fenrg.2014.00009

4. Wang X, Si X, Li C, Guo X, Cao J. Joining the $BaZr_{0.1}Ce_{0.7}Y_{0.1}Yb_{0.1}O_{3-\delta}$ electrolyte to AISI 441 interconnect for protonic ceramic fuel cell applications: interfacial microstructure and long-term stability, ACS Appl Energy Mater. 2021;4:7346–7354. doi:10.1021/acsaem.1c01491

5. He F, Teng Z, Yang G, Zhou C, Guan D, Chen S, Ran R, Wang W, Zhou W, Shao Z. Manipulating cation nonstoichiometry towards developing better electrolyte for self-humidified dual-ion solid oxide fuel cells. J Power Sources. 2020;460:228105. doi:10.1016/j.jpowsour.2020.228105

6. Liu Z, Chen Y, Yang G, Yang M, Ji R, Song Y, Ran R, Zhou W, Shao Z. One-pot derived thermodynamically quasi-stable triple conducting nanocomposite as robust bifunctional air electrode for reversible protonic ceramic cells. Appl Catal B Environ. 2022;319:121929. doi:10.1016/j.apcatb.2022.121929

7. Wan Y, He B, Wang R, Ling Y, Zhao L. Effect of co doping on sinterability and protonic conductivity of $BaZr_{0.1}Ce_{0.7}Y_{0.1}Yb_{0.1}O_{3-\delta}$ for protonic ceramic fuel cells. J Power Sources. 2017;347:14–20. doi:10.1016/j.jpowsour.2017.02.049

8. Yang S, Zhang S, Sun S, Ye X, Wen Z. Lattice incorporation of Cu^{2+} into the $BaCe_{0.7}Zr_{0.1}Y_{0.1}Yb_{0.1}O_{3-\delta}$ electrolyte on boosting its sintering and protonconducting abilities for reversible solid oxide cells. ACS Appl Mater Interfaces. 2018;10:42387–42396. doi:10.1021/acsami.8b15402

9. Zhang Y, Xie D, Chi B, Pu J, Li J, Yan D. Basic properties of proton conductor $BaZr_{0.1}Ce_{0.7}Y_{0.1}Yb_{0.1}O_{3-\delta}$ (BZCYYb) material. Asia-Pacific J Chem Eng. 2019;14(4):e2322. doi:10.1002/apj.2322

10. Hamze L, Suard E, Joubert O, Quarez E. Synthesis and temperature dependence of the crystal structure of proton conductor $BaZr_{0.1}Ce_{0.7}Y_{0.1}Yb_{0.1}O_{3-\delta}$ (BZCYYb1711) by combined neutron and X-ray diffraction. Solid State Ionics. 2024;417:116682. doi:10.1016/j.ssi.2024.116682

11. Sereda V, Tsvetkov D, Malyshkin D, Ivanov I, Sednev-Lugovets A, Zuev A. Hydration-induced chemical expansion of $BaCa_{(1+y)/3}Nb_{(2-y)/3}O_{3-\delta} \cdot xH_2O$ (BCN) and other proton-conducting perovskite oxides. Solid State Ionics. 2020;358:115516. doi:10.1016/j.ssi.2020.115516